Paclitaxel-induced epithelial damage and ectopic MMP-13 expression promotes neurotoxicity in zebrafish

Thomas S. Lisse[a,1], Leah J. Elias[a], Adriana D. Pellegrini[a], Paige B. Martin[a], Emily L. Spaulding[a], Olivia Lopes[a], Elizabeth A. Brochu[a], Erin V. Carter[a], Ashley Waldron[a], and Sandra Rieger[a,2]

[a]Kathryn W. Davis Center for Regenerative Biology and Medicine, MDI Biological Laboratory, Salisbury Cove, ME 04672

Edited by Thomas C. Südhof, Stanford University School of Medicine, Stanford, CA, and approved February 26, 2016 (received for review December 21, 2015)

Paclitaxel is a microtubule-stabilizing chemotherapeutic agent that is widely used in cancer treatment and in a number of curative and palliative regimens. Despite its beneficial effects on cancer, paclitaxel also damages healthy tissues, most prominently the peripheral sensory nervous system. The mechanisms leading to paclitaxel-induced peripheral neuropathy remain elusive, and therapies that prevent or alleviate this condition are not available. We established a zebrafish in vivo model to study the underlying mechanisms and to identify pharmacological agents that may be developed into therapeutics. Both adult and larval zebrafish displayed signs of paclitaxel neurotoxicity, including sensory axon degeneration and the loss of touch response in the distal caudal fin. Intriguingly, studies in zebrafish larvae showed that paclitaxel rapidly promotes epithelial damage and decreased mechanical stress resistance of the skin before induction of axon degeneration. Moreover, injured paclitaxel-treated zebrafish skin and scratch-wounded human keratinocytes (HEK001) display reduced healing capacity. Epithelial damage correlated with rapid accumulation of fluorescein-conjugated paclitaxel in epidermal basal keratinocytes, but not axons, and up-regulation of matrix-metalloproteinase 13 (MMP-13, collagenase 3) in the skin. Pharmacological inhibition of MMP-13, in contrast, largely rescued paclitaxel-induced epithelial damage and neurotoxicity, whereas MMP-13 overexpression in zebrafish embryos rendered the skin vulnerable to injury under mechanical stress conditions. Thus, our studies provide evidence that the epidermis plays a critical role in this condition, and we provide a previously unidentified candidate for therapeutic interventions.

MMP-13 | degeneration | regeneration | Taxol | epidermis

Paclitaxel is a microtubule-stabilizing chemotherapeutic agent that is widely used in the treatment of common cancers, including breast, ovarian, and lung cancer. Despite its promising anticancerous properties, paclitaxel also damages healthy tissues, most prominently peripheral axons of somatosensory neurons (reviewed in ref. 1). Paclitaxel-induced peripheral neuropathy initiates in the distal extremities and presents as neuropathic pain syndrome, temperature sensitivity, and paresthesia (tingling and numbness). Nerve biopsies from patients suggest that axon degeneration is the primary manifestation of this condition, followed by secondary demyelination and nerve fiber loss in severely affected patients (1, 2). Certain drugs have been shown in vitro and in vivo to protect against paclitaxel-induced nerve damage, including acetyl-L-carnitine, erythropoietin, alpha-lipoic acid, olesoxime, amifostine, nerve growth factor, and glutamate (reviewed in ref. 3). However, so far, these agents have either not successfully passed clinical trials or merely alleviate symptoms such as pain without prevention (1). Thus, a better understanding of the underlying causes of paclitaxel-induced peripheral neuropathy is necessary and may help identify new candidate drugs with which to treat this condition.

A widely accepted mechanism for paclitaxel neurotoxicity is the "dying back" of distal nerve endings (4), which has been attributed to aberrant axonal microtubule transport and cytoplasmic flow, as well as mitochondrial defects, both shown in vivo and in vitro (5–7). In vitro studies further demonstrated that paclitaxel induces axon degeneration upon direct application to axons (8), and thus a general thought is that paclitaxel-induced axon damage is largely neuron-autonomous. Whether these observations reflect the in vivo effects of paclitaxel remains to be shown, however. The specificity of paclitaxel-induced axon degeneration, which initiates in intraepidermal A- and C-fibers of dorsal root ganglion (DRG) neurons innervating the glabrous skin of palm and sole (9–11), suggests that environmental factors could play a critical role. The palms and soles are more frequently injured and exposed to biomechanical stresses, and cutaneous axons, for instance, are receptive to mechanical stress through binding via integrin receptors to the extracellular matrix (ECM) (12). Moreover, sensory axons and keratinocytes are in close apposition (13, 14) and have been shown to communicate through various molecular mechanisms. For instance, after injury keratinocytes promote axon regeneration by secreting hydrogen peroxide (H_2O_2) (15). On the other hand, cutaneous axons secrete neuropeptides to promote cutaneous homeostasis (16). Intriguingly, epithelial cells are highly susceptible to paclitaxel-induced damage, evident by the efficacy of paclitaxel in the treatment of carcinomas and by its skin-damaging effects in humans (10)

Significance

Paclitaxel is a widely used chemotherapeutic agent in the treatment of cancer. Although paclitaxel arrests tumor growth through stabilizing microtubules, it also causes variable peripheral neuropathy in patients. A lack of understanding of the underlying mechanisms hinders therapeutic discovery, and commonly used mammalian models have not provided conclusive evidence about the etiology of this condition. To overcome this, we developed a larval zebrafish model that permits the analysis of paclitaxel neurotoxicity in living animals. This study identifies that keratinocyte damage and ectopic expression of matrix-metalloproteinase 13 (MMP-13) contributes to paclitaxel-induced peripheral neuropathy in zebrafish. We further show that inhibition of MMP-13 improves skin defects and prevents paclitaxel neurotoxicity. Thus, this study offers a previously unidentified avenue for potential therapeutic interventions.

Author contributions: S.R. designed research; T.S.L., L.J.E., A.D.P., P.B.M., E.L.S., O.L., E.A.B., E.V.C., A.W., and S.R. performed research; S.R. contributed new reagents/analytic tools; T.S.L., L.J.E., and S.R. analyzed data; and S.R. wrote the paper.

The authors declare no conflict of interest.

This article is a PNAS Direct Submission.

Freely available online through the PNAS open access option.

[1]Present address: The Jackson Laboratory, Bar Harbor, ME 04609.

[2]To whom correspondence should be addressed. Email: srieger@mdibl.org.

This article contains supporting information online at www.pnas.org/lookup/suppl/doi:10.1073/pnas.1525096113/-/DCSupplemental.

and cell culture (17). Therefore, perturbations of the skin environment by paclitaxel treatment could promote axon degeneration, yet no studies to date have examined this possibility. We have established a zebrafish in vivo model to study paclitaxel's neurotoxic effects in live animals. These studies demonstrate that paclitaxel promotes epidermal damage and neurotoxicity and induces keratinocyte-specific up-regulation of matrix-metalloproteinase 13 (MMP-13, collagenase 3). Pharmacological inhibition of MMP-13 rescues paclitaxel-induced neurotoxicity, making it a previously unidentified therapeutic candidate.

Results

Paclitaxel Induces Neurotoxicity in the Zebrafish Caudal Fin. To assess peripheral neuropathy in adult zebrafish, we administered up to 0.133 mg/kg paclitaxel in DMSO by i.p. injections on 4 consecutive days. Because paclitaxel preferentially affects the distal extremities in mammals, we analyzed the equivalent distal caudal fin in zebrafish. Immunofluorescence staining 1 d after the last injection (day 4) using anti-acetylated tubulin (Fig. 1 *B* and *C* and Movies S1 and S2) and Neurofilament 160 (Fig. S1) antibodies revealed a selective loss of fine cutaneous fibers and axons projecting along the bony rays within the distal, but not proximal, fin regions. Three distinct neuronal populations innervate the caudal fin. DRG axons project into the distal fin, whereas motor axons project into the proximal fin. Lateral line axons innervate neuromasts along the bony rays. Because primarily fine cutaneous axons were lost in the distal-most fin region, we conclude that paclitaxel treatment primarily affects DRG axons. To further corroborate this, we also examined temporal changes in the touch response, which we expected to be attenuated if cutaneous axons are lost (Fig. 1*A*). This showed that paclitaxel-treated animals needed significantly more stimulations at the distal fin before a twitching response was evoked compared with controls (Fig. 1*D*). We next determined the effects of paclitaxel on swimming behavior, given that in mammals high doses of paclitaxel have been associated with motor deficits. Using an automated tracking device, we measured daily 1-h swimming distances, which did not show significant differences (Fig. 1*E*). These findings indicate that paclitaxel specifically damages DRG axons within the distal caudal fin.

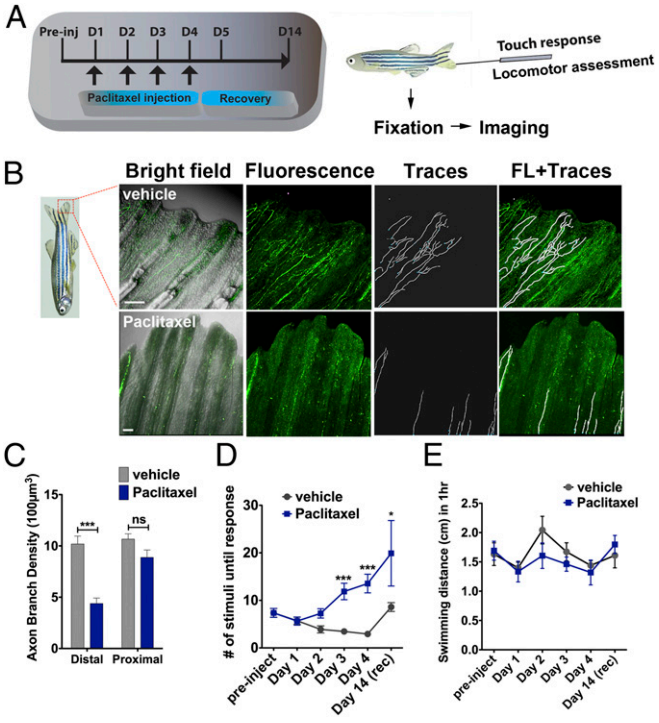

Fig. 1. Paclitaxel induces sensory axon degeneration and loss of touch response in adult zebrafish. (*A*) Experimental design for induction and assessment of peripheral neuropathy in adult zebrafish by daily injections of 10 μM paclitaxel on 4 consecutive days, followed by 10 d of recovery. (*B*) Anti-acetylated tubulin staining of axons 1 d after the last injection. Fine cutaneous nerve endings are present in vehicle control (*Top*) but not in paclitaxel-treated (*Bottom*) fish. Vehicle axons were partially traced. (Scale bar, 100 μm.) (*C*) Selective nerve fiber loss in distal but not proximal caudal fin ($n = 7$, 5–6 fish per group). (*D*) Touch response assessed before each daily injection and during a recovery period reveals a significantly delayed response after four injections (day 3) ($n = 7$, 5–12 fish per group), which leads to variable recovery by day 14 ($n = 2$, 5 fish). (*E*) One-hour swimming distances are not significantly different between vehicle and paclitaxel-treated fish ($n = 2$, 5 fish per group). $^{*}P < 0.05$, $^{**}P < 0.01$, $^{****}P < 0.0001$. D, day; FL, fluorescence; preinj, preinjection day; rec, recovery.

We next investigated axon degeneration in zebrafish larvae using in vivo imaging to obtain a higher temporal resolution. In larval fish [up to 26 d postfertilization (dpf)], the skin consists of two layers: the superficial periderm of ectodermal origin and the epidermal basal cell layer (18, 19). The epidermis is separated from the underlying rudimentary dermis by a basement membrane. DRG neurons are not functional until ∼4 wk when the epidermis stratifies, and initially axons of unmyelinated Rohonbeard (RB) neurons with analogy to mammalian C-fibers (20) innervate the skin and arborize between both layers. To assess RB axon degeneration in transgenic Tg(*isl2b*:GFP) (21) (Fig. 2*B*) larvae with fluorescently labeled sensory neurons, we incubated them in 22 μM paclitaxel starting at 2 dpf. This showed that a 96-h treatment (2–6 dpf) resulted in significant axon degeneration (Fig. 2 *A* and *C*–*E*). Incubated larvae had a slightly decreased caudal fin diameter (Fig. S2), which was not caused by increased apoptosis (Fig. S3), suggesting that paclitaxel slows developmental growth. We next assessed the touch response (Fig. 2*F*), which was significantly reduced starting 1 d after treatment began. In contrast, no defects were seen in locomotor activity (Fig. 2*G*). We next analyzed paclitaxel-dependent axon damage following injections into the cardinal vein once daily on 3 consecutive days using 10 μM paclitaxel (Fig. 2*H*), as this concentration has also been used in various mammalian models (22). Microinjections similarly induced axon degeneration (Fig. 2*I*) and reduced touch sensitivity (Fig. 2*J*). Both were prominent after the last injection and rapidly recovered thereafter. It is noteworthy that at 11 dpf both control and paclitaxel-injected larvae harbored fewer axon branches, likely due to the onset of programmed RB neuron death (23). Collectively, these findings show that paclitaxel also induces RB neurotoxicity in larval fish without affecting locomotor activity.

Paclitaxel Damages the Fin Epithelium Before Onset of Axon Degeneration. We noticed that the morphology of the caudal fin-fold in paclitaxel-injected larvae was altered as early as 1 h after injection (Fig. 3 *A*–*C* and Fig. S4). Caudal fins had a disheveled appearance and were often injured due to mechanical stress during handling of larvae (Fig. 3*D*). Scanning electron microscopy (SEM) showed an increased number of microtears in the distal caudal fin following 3 h of paclitaxel treatment (Fig. 3 *E* and *F*). This phenotype worsened in larvae treated with paclitaxel for 96 h, evident by delamination of keratinocytes from both layers and exposure of collagen-rich actinotrichia in the mesenchyme beneath. Also the adult skin displayed paclitaxel-induced morphological changes assessed with a green fluorescent ceramide membrane stain. The cells appeared disorganized and rounded compared with the cuboidal shape of control cells (Fig. S5). These findings indicate that paclitaxel damages the skin epithelium, making the skin less resistant to mechanical stress and prone to injury.

To further investigate the role of mechanical stress in paclitaxel-induced epithelial damage, we assessed the formation of

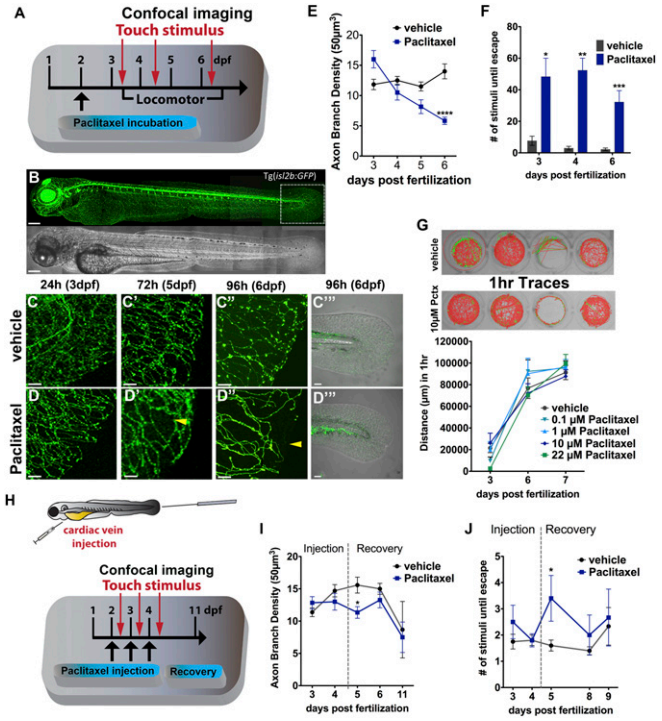

Fig. 2. Paclitaxel induces neurotoxicity in larval zebrafish. (*A*) Scheme of larval paclitaxel (22 μM) incubation and assessment of neuropathy. (*B*) Image assembly of Tg(*isl2b*:GFP) zebrafish strain used to analyze axon degeneration in *C–E*, and *I*. (Scale bar, 200 μm.) (*C* and *D*) Axon branches in caudal fins of vehicle- (*C*) and paclitaxel- (*D*) treated larvae after 24, 72, and 96 h (*C–D″*). (Scale bar, 20 μm.) Bright field images of fin after 96 h of treatment (*C‴* and *D‴*). [Scale bar, 50μm (*E*).] Reduced axon branch density after 96 h of paclitaxel treatment ($n = 3$, 5–7 larvae per group). (*F*) More touch stimuli are required to evoke a response in paclitaxel-treated larvae ($n = 3$, 10–15 larvae per group). (*G*, *Upper*) One-hour sample traces of single vehicle and paclitaxel-treated larvae in each well. Green tracks indicate normal and orange above threshold speed. (*G*, *Bottom*) No significant difference in swimming distance ($n = 2$, 8 fish per group). (*H*) Scheme of paclitaxel (10 μM) microinjections and axon and behavioral analyses. (*I*) Axon branch density is significantly reduced after three injections and rapidly recovers. Note that the axon branch density at 11 dpf has also decreased in controls, as the RB neuron population diminishes ($n = 3$, 8 fish per group). (*J*) Touch response is transiently delayed after the third injection and restored during recovery ($n = 3$, 5 fish per group). $^*P < 0.05$, $^{**}P < 0.01$, $^{****}P < 0.0001$. dpf, days postfertilization.

reactive oxygen species (ROS) in the caudal fin of mechanically stressed animals using a H_2O_2-selective sensor. Three-hour paclitaxel treatment followed by gentle pipetting led to more widespread ROS/H_2O_2 formation compared with control animals (Fig. 3*G*). Intriguingly, adjacent wounds remained devoid of ROS/H_2O_2, suggesting that stress-related ROS formation may be regulated by different mechanisms than injury-induced ROS. Given the stress responses, we next examined the NF-κB stress response pathway in a transgenic Tg(NF-κB:EGFP) reporter strain (24), which shows NF-κB activation in keratinocytes (Fig. S6). NF-κB was activated in keratinocytes by paclitaxel but not vehicle treatment under both unstressed and mechanically stressed conditions (Fig. 3 *H* and *I*). Because NF-κB is known to be regulated by H_2O_2 (25), we also assessed the relationship between NF-κB activity and ROS/H_2O_2 formation with the superoxide scavenger diphenyleneiodonium (DPI) and apocynin, a bona fide NOX inhibitor, both of which attenuated NF-κB activity (Fig. 3*I*). These findings suggest that NF-κB activation in keratinocytes is in part mediated by paclitaxel-induced oxidative stress.

The rapid phenotypic changes in the larval caudal fin suggested that the epithelium might be more susceptible to paclitaxel-induced damage than RB neurons. To test this, we tracked paclitaxel accumulation in the fin epithelium and in RB neurons of transgenic Tg(CREST3:tdTomato) larvae during 12-h time-lapse recordings (Fig. 3 *J–L*) using tubulin tracker, a paclitaxel conjugate to Oregon Green 488, which selectively binds to microtubules with high affinity ($K_d \sim 10^{-7}$) (26) and which fluoresces upon cleavage by intracellular esterases. Following normalization, we observed a transient fluorescence increase in the caudal fin within 3 h (Fig. 3 *J* and *K*), whereas neuronal fluorescence peaked around 5–8 h and was only present in some, but not all, RB neurons (Fig. 3*L*). To further determine whether tubulin tracker within the caudal fin accumulated in keratinocytes and/or RB axons, we performed colocalization studies in animals either transiently injected with CREST3:tdTomato to label axons in red or animals transgenic for basal keratinocyte-specific dsRed expression [Tg(*tp63*:dsRed)]. Although we did not detect tubulin tracker in axons up to 12 h following injections (Fig. 3*M* and Movie S3), we found its rapid accumulation in basal keratinocytes (Fig. 3*N* and Movie S4). Interestingly, only basal but not periderm cells showed tubulin tracker accumulation. Together, these findings indicate that basal keratinocytes are more susceptible to paclitaxel accumulation compared with RB neurons and their cutaneous axons.

Paclitaxel Impairs Cutaneous Axon Regeneration. We previously demonstrated that epithelial keratinocytes stimulate cutaneous axon regeneration through release of H_2O_2 into the wound environment (15), and our observations showed that H_2O_2 production is impaired in wounds of paclitaxel-treated larvae (Fig. 3*G*). We therefore hypothesized that axon regeneration might be impaired, possibly due to perturbed keratinocyte function. To assess this, we first tracked the mean growth of single-labeled RB axons for 12 h following caudal fin amputation during which animals remained in vehicle or paclitaxel solution (Fig. 4 *A–C*). This showed that paclitaxel significantly impaired axon regeneration (Movies S5 and S6). We wanted to further analyze how paclitaxel influences growth cone behavior, as the growth cone core domain of regenerating axons is rich in dynamically instable microtubules that allow growth and shrinkage of axons (27), which could be stabilized by paclitaxel. Such growth and retraction behavior is also characteristic for RB axons (15). Quantification of total growth and retraction over the course of 12 h revealed that paclitaxel attenuated, but did not abolish, this process (Fig. 4*D*). Because lack of growth could also relate to defects mediated within the epidermis due to keratinocyte damage, we next assessed paclitaxel's effects on Wallerian degeneration (WD), for which it was shown in *Drosophila* and zebrafish that axon debris clearance depends on keratinocytes acting as "nonprofessional" phagocytes (28, 29). Similar to mammals, zebrafish cutaneous axons degenerate by WD when severed (30), a process that is defined by a lag phase during which the severed axons remain intact, an axon fragmentation phase, and a clearance phase during which axon debris is phagocytosed. Paclitaxel did not interfere with the ability of axons to fragment; however, the duration of clearance was altered. The time between fragmentation onset of individual axon branches and complete clearance of axon debris was twice as long for paclitaxel-treated compared with vehicle-treated controls (Fig. 4 *A*, *B*, and *E*). These findings suggest that paclitaxel may exert its effects on axon regeneration through damaging keratinocytes.

MMP-13 Inhibition Partially Rescues Impaired Axon Regeneration. We exploited our zebrafish model to screen for chemical compounds that can restore impaired axon regeneration and debris clearance in the presence of paclitaxel. We used preselected compounds targeting proteins of genes that we found were differentially

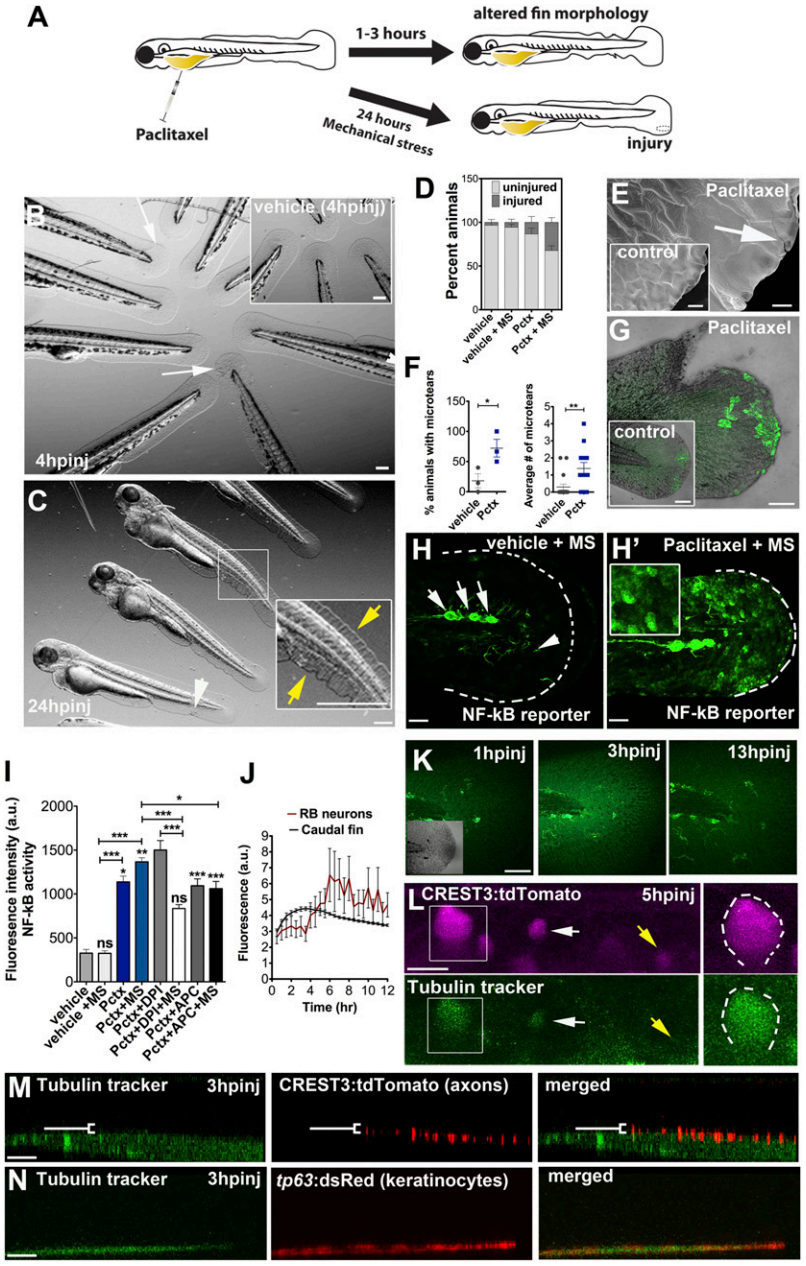

Fig. 3. Paclitaxel-induced epithelial damage precedes cutaneous axon degeneration. (*A*) Scheme of caudal fin phenotypes observed within 3 h after paclitaxel injection in the presence or absence of mechanical stress. (*B*) Altered fin morphology (arrows) 4 h after paclitaxel injection (*Inset* shows vehicle-injected controls). (Scale bar, 200 μm.) (*C*) Disheveled fin-fold (yellow arrows) and skin injury (white arrow) after 24 h. *Inset* shows higher magnification of boxed region. (Scale bar, 200 μm.) (*D*) Increased injury formation 24 h after paclitaxel injection, which is exacerbated by mechanical stress (MS) ($n = 3$, 5 larvae per group). (*E*) Scanning electron micrographs of distal caudal fins following 3 h of incubation in vehicle (*Inset*) or paclitaxel. Paclitaxel animal with microtear (arrow) indicates brittle skin. (Scale bar, 10 μm.) (*F*) Percent of animals with microtears (*Left*) and average number of microtears per animal (*Right*; as shown in *E*) are increased after 3 h of paclitaxel treatment. (*G*) Increased ROS/H_2O_2 detection ($n = 5$ per group) with pentafluorobenzenesulfonyl-fluorescein in the caudal fin of paclitaxel-treated, stressed animals, not seen in the injury site, or in stressed vehicle controls (*Inset*). (Scale bar, 50 μm.) (*H* and *H'*) NF-κB reporter activity after mechanical stress is restricted to neuromasts (white arrows) and dendritic cells (white arrowhead) in control larva (*H*) and also found in keratinocytes of paclitaxel-treated larva (*H'*) (*Inset* shows higher magnification of keratinocytes; see also Fig. S6). (Scale bar, 50 μm.) (*I*) NF-κB reporter activity with and without H_2O_2 scavengers in vehicle and paclitaxel-treated stressed and unstressed larvae ($n = 3$, 3–6 fish per group; $^*P < 0.05$ and $^{***}P < 0.001$). (*J*) Tubulin tracker fluorescence increase in caudal fin peaks around 3 h post-injection (hpinj) and around 5 hpinj in RB neuron cell bodies, shown in *K* and *L* ($n = 3$, 4 fish per group). (*K*) Tubulin tracker (10 μM) in caudal fin at 3 h following injection. (Scale bar, 100 μm.) (*L*) Tubulin tracker is present in large (boxed) and small (white arrow) diameter RB neuron cell bodies at 5 hpinj. Note that not all neurons accumulate tubulin tracker (yellow arrow). (Scale bar, 10 μm.) (*M*) Tubulin tracker does not colocalize with cutaneous axons at 3 hpinj [white bracket indicates axons (red) above tubulin tracker-positive basal layer]. (Scale bar, 10 μm.) (*N*) Tubulin tracker colocalizes with basal keratinocytes (red) at 3 hpinj. (Scale bar, 10 μm.) APC, apocynin; DPI, diphenyleneiodonium; hpinj, hours postinjection; MS, mechanically stressed; Pctx, paclitaxel.

regulated in H_2O_2-treated larval zebrafish following RNAseq analysis (Fig. 4*F*) (31). Each compound was coadministered with paclitaxel for 12 h during time-lapse recordings. This screen identified one compound, CL-82198 (10 μM) (Fig. 4*G*), for improving axon regeneration (Fig. 4*C*). CL-82198 is a MMP-13 inhibitor and displays no activity against MMP-1 or MMP-9 (32). Its efficacy in humans is currently unknown. To confirm MMP-13 as a target, we tested another selective, non–zinc-chelating MMP-13 inhibitor, DB04760 (33) (Fig. 4*G*), which also significantly rescued axon regeneration (Fig. 4*C* and Movie S7) and axon debris clearance (Fig. 4 *E* and *H*). We next assessed whether MMP-13 inhibition attenuates paclitaxel neurotoxicity by analyzing axon branch density and touch response following 96 h of incubation. Intriguingly, both inhibitors, when coadministered with paclitaxel, prevented axon degeneration (Fig. 4*I*) and also largely restored the touch response, with DB04760 being more efficient than CL-82198 (Fig. 4*J*). Only ∼30% of larvae treated with paclitaxel + CL-82198 were unresponsive to touch, as opposed to ∼50% when treated with paclitaxel (Fig. 4*K*), suggesting that a subset of animals benefited from this compound. Continuous CL-82198 but not DB04760 coadministration for 4 d showed some adverse effects, evident by a decreased response when stimulated in the head beneath the eyes, which served as the control region. Head stimulation evoked, however, wild type-like responses when either CL-82198 or DB04760 were administered alone (Fig. S7). Also adult fish greatly benefited from DB04760 and CL-82198 coadministration, evident by an improved touch response and axon branch number assessed 1 d (Fig. 5 *A* and *B* and Fig. S8) and 10 d (day 14) (Fig. 5*C*) after the last injection. It is noteworthy that both MMP-13 inhibitors improved overall health of adult fish, evident by decreased lethality after accidental injury. Interestingly, the axon branch density in paclitaxel-treated fish only slightly increased by day 14, consistent with a persistent overall insensitivity to touch. These findings demonstrate that DB04760 and CL-82198 greatly reduce neurotoxicity associated with paclitaxel treatment in larval and adult zebrafish.

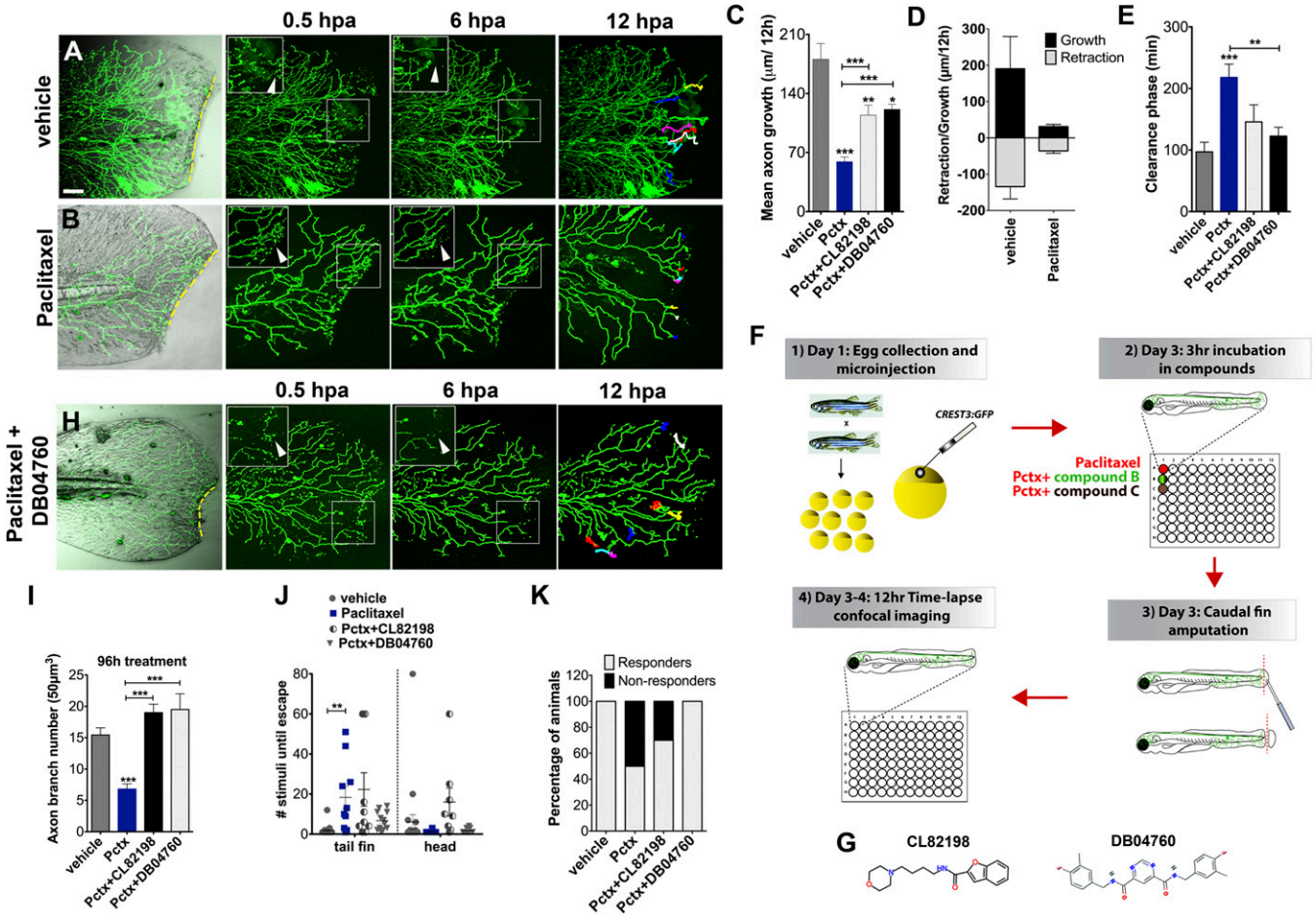

Fig. 4. Paclitaxel-induced neurotoxicity in larval fish is attenuated by MMP-13 inhibition. (*A* and *B*) Cutaneous branches of a single-labeled RB neuron were traced for 12 h in the caudal fin following fin amputation. Larvae were incubated for 3 h either in vehicle solution (0.5% DMSO/Ringers) (*A*) or paclitaxel (22 μM) (*B*). *Insets* show higher magnification of boxed regions (arrowheads depict axon debris lost in vehicle but not paclitaxel-treated animals). Tracks in the last panel depict branch growth over time. (*C*) Quantification of mean axon branch growth over 12 h in larvae incubated in vehicle, paclitaxel (22 μM), and paclitaxel plus either DB04760 or CL-82198 (10 μM each) ($n = 3$, 3–4 fish per group). (*D*) Comparison of mean axon growth and retraction in injured vehicle and paclitaxel-treated animals over 12 h ($n = 2$, 3–4 fish and 15 axons per group). (*E*) Quantification of axon debris clearance ($n = 2$, 3–4 fish and 5–7 axons per group). (*F*) Scheme of compound screening assay. (*G*) Chemical structures of MMP-13 inhibitors. CL-82198, *N*-[4-(4-morpholinyl)butyl]-2-benzofurancarboxamide; DB04760, N4,N6-bis[(4-fluoro-3-methylphenyl)methyl] pyrimidine-4,6-dicarboxamide. (*H*) Axon regeneration is partially restored with 10 μM DB04760 (arrowheads mark diminishing axon debris). (*I*) Comparison of axon branch density following 96 h of treatment ($n = 2$, 5 fish per group). (*J*) Touch response in fin and head region after 96 h of treatment ($n = 4$, 5 fish per group). (*K*) Percentage of animals with improved touch response upon coadministration of paclitaxel and either CL-82198 or DB04760. $^*P < 0.05$, $^{**}P < 0.01$, $^{***}P < 0.001$. (Scale bar, 50 μm.) hpa, hours postamputation; Pctx, paclitaxel.

Paclitaxel Induces Ectopic MMP-13 Expression. MMP-13 is expressed at relatively low levels in the uninjured skin epithelium but is up-regulated in response to acute tissue injury (34, 35) where it is essential for proper wound repair (36). On the contrary, increased MMP-13 activity in uninjured tissues can promote injury (37) and cancer metastasis (38), suggesting that precisely controlled levels are essential for tissue homeostasis. We hypothesized that paclitaxel induces ectopic MMP-13 expression within the skin, consistent with the beneficial effects of the inhibitors. To test this, we determined mRNA expression levels of the zebrafish MMP-13 homolog *mmp13a* with quantitative PCR (qPCR) following 3 h of paclitaxel incubation. Transcript levels were elevated in uninjured paclitaxel but not vehicle-treated larvae and were enhanced upon amputation (Fig. 6*A*). MMP-13 exists as both an uncleaved (proenzyme) and cleaved active form. Various isoforms were reported, including 35, 48, and 54 kDa for the active and 60 and 80 kDa for the proenzyme (39), likely depending on species, age, and tissue types analyzed. Western analysis following 3 h of treatment revealed expected bands at 48 and 54 kDa for the cleaved and 80 kDa for the proenzyme (Fig. 6*B*). Quantifications revealed that the intermediate 54 kDa, but not 48 kDa, isoform was more abundant in paclitaxel-treated larvae compared with the respective vehicle control groups (Fig. 6 *C* and *D*).

Given the preferential accumulation of tubulin tracker in basal keratinocytes, we hypothesized that MMP-13 is up-regulated in keratinocytes. To test this, we used whole-mount immunofluorescence staining. In mice, MMP-13 has been detected in dermal fibroblasts of skin wounds (40) and in the leading edge of migratory epithelial cells following corneal injury (41). In zebrafish embryos, *mmp13a* was detected after caudal fin amputation (35), and we also detected MMP-13 specifically at the amputation wound of larvae (Fig. 6 *E*–*E*″). Paclitaxel treatment enhanced MMP-13 expression, showing a uniform staining within the caudal fin (Fig. 6 *F*–*F*″, *G*, and *H* and Movie S8) but not within RB axons (Fig. 6 *I*–*K*″ and Movie S9). Intriguingly, similar to tubulin tracker, MMP-13 expression was also localized to basal keratinocytes (Fig. 6 *L*–*L*″). In the adult distal caudal fin, MMP-13 expression was found in the dermis of both vehicle and paclitaxel-treated animals but was specifically up-regulated in basal cells after paclitaxel treatment (Fig. 5 *D* and *E*). MMP-13 staining

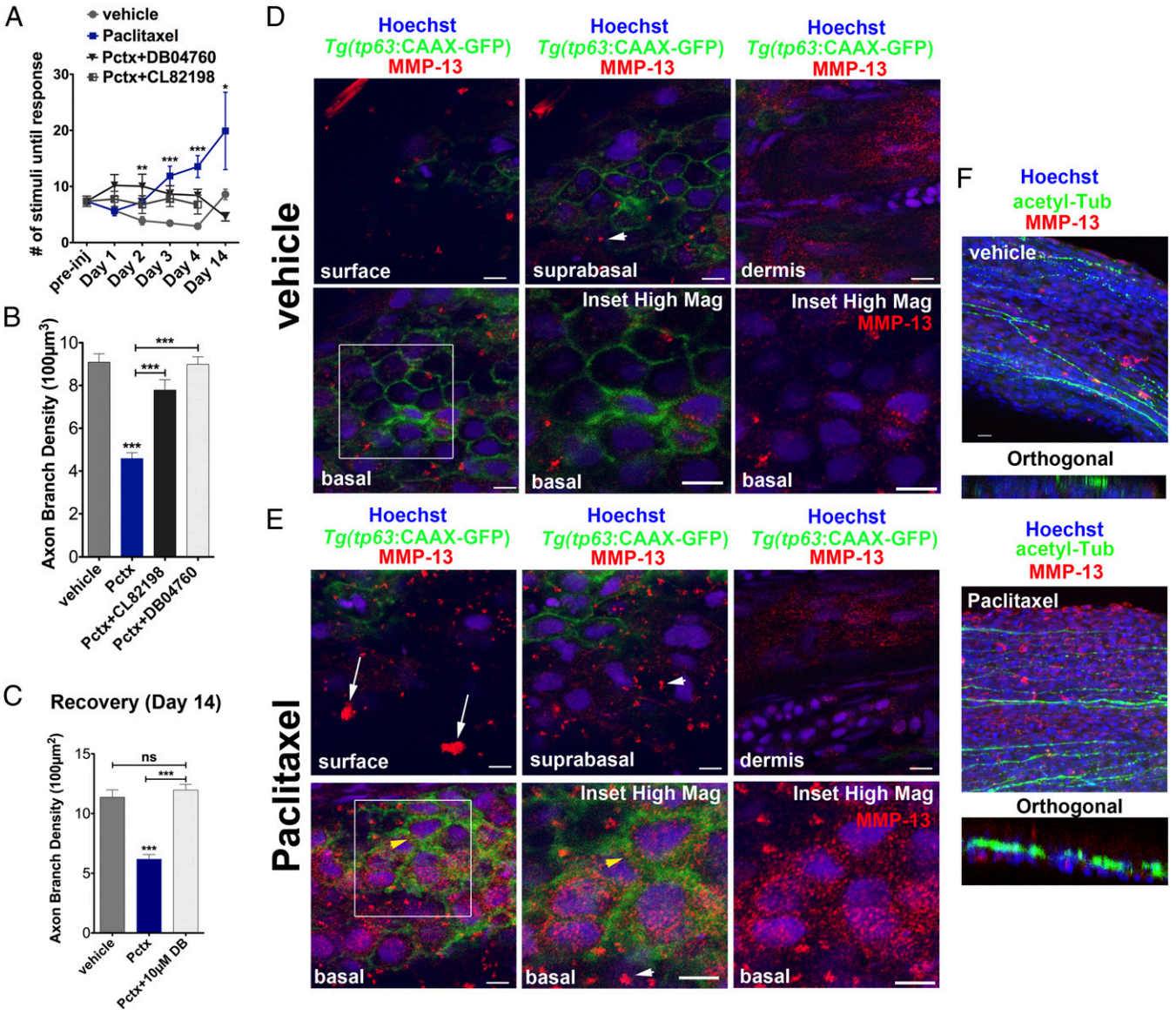

Fig. 5. MMP-13 inhibition improves adult paclitaxel-induced neurotoxicity. (*A*) Improved touch response upon coadministration of paclitaxel and either DB04760 or CL-82198 following four injections ($n = 7$, 7–12 fish per group) and complete rescue by day 14 in DB04760 coadministered animals ($n = 2$, 5 fish). (*B* and *C*) Axon branch density in distal caudal fin is rescued upon coadministration of paclitaxel and either DB04760 or CL-82198 when assessed 1 d (*B*) ($n = 3$, 7–12 fish per group) or 10 d (*C*) ($n = 2$, 5 fish per group) after the last injection. (*D* and *E*) MMP-13 immunofluorescence staining (red) 1 d after the last injection shows MMP-13 up-regulation specifically in basal keratinocytes (yellow arrowheads) of Tg(*tp63*:CAAX-GFP) fish injected with paclitaxel (*E*) and low MMP-13 expression in vehicle controls (*D*). Imaging was performed using identical settings. Dermal cells in both vehicle and paclitaxel-injected fish have similar MMP-13 expression levels. White arrowheads depict large distinctive MMP-13 clusters. (*E*) White arrows depict clusters of MMP-13–positive cellular debris at the skin surface, indicative of increased cell shedding. (Scale bar, 5 µm.) (*F*) MMP-13 staining (red) is adjacent to, but not within, DRG axons (green). (Scale bar, 10 µm.) $*P < 0.05$, $***P < 0.001$, $****P < 0.0001$. ac-tub, acetylated tubulin; Pctx, paclitaxel.

was adjacent to, but not within, DRG axons (Fig. 5*F*). Interestingly, although MMP-13 expression showed an even punctate pattern in the basal layer, we also found distinct clusters in both the basal and suprabasal layer (Fig. 5*E*, arrowheads), which were largely absent in vehicle controls (Fig. 5*D*, arrowheads). At the surface of the skin, MMP-13 was clustered within dead cells seen after paclitaxel but not vehicle treatment (Fig. 5*E*, arrows). Collectively, these findings suggest that paclitaxel up-regulates MMP-13 expression in epidermal keratinocytes but not within cutaneous axons.

MMP-13 Up-Regulation Impairs Epithelial Barrier Function and Reduces Mechanical Stress Resistance. Increased MMP-13 activity has been linked to defects in epithelial barrier function, such as in the gut epithelium, where it destabilizes tight junctions (TJs) (42). We therefore assessed whether paclitaxel-dependent MMP-13 up-regulation promotes skin barrier defects. We previously showed that H_2O_2 diffuses into the larval skin, evident by its ability to induce RB axon growth in uninjured animals (15). We hypothesized that barrier defects will enhance diffusion of exogenous H_2O_2 into the skin. To quantitatively assess this, we generated transgenic Tg(*krt4*:HyPer) zebrafish larvae expressing the ratiometric, genetic H_2O_2 sensor HyPer in keratinocytes. The submicromolar affinity of HyPer for H_2O_2 and its insensitivity to other ROS permits the detection of small changes in H_2O_2 concentrations. We found that the mean HyPer ratio following

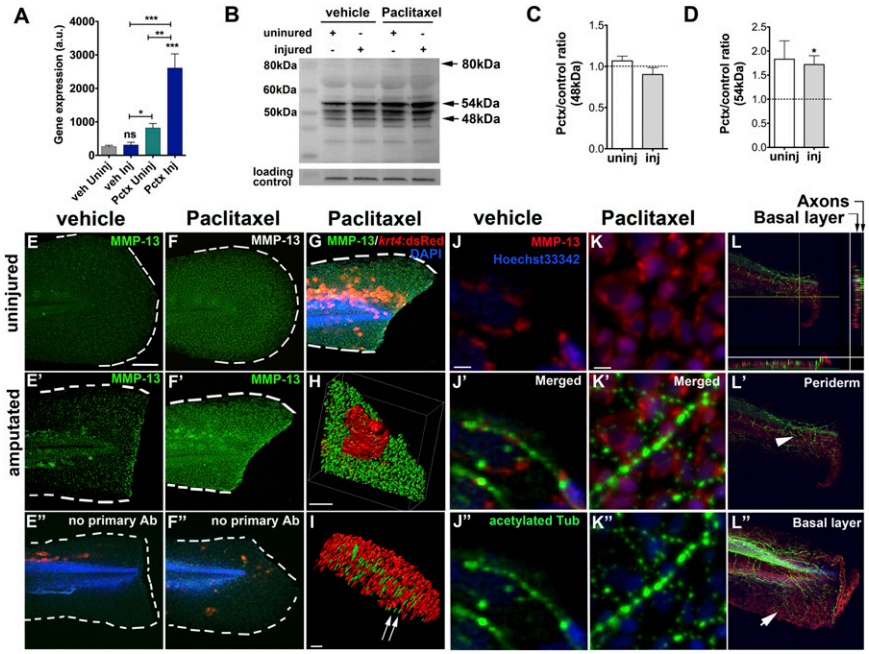

Fig. 6. Paclitaxel stimulates MMP-13 expression. (*A*) Quantitative real-time PCR shows increased *mmp13a* expression in uninjured and injured animals treated with 22 μM paclitaxel for 3 h (15 pooled larvae per group). (*B*) Western analysis shows higher abundance of the 54-kDa isoform in uninjured and injured animals treated with paclitaxel for 3 h (10 pooled larvae per group). (*C* and *D*) Paclitaxel/vehicle ratios for normalized 48-kDa (*C*) and 54-kDa (*D*) bands in uninjured and injured animals (n = 2, 10 pooled larvae). Dashed lines demarcate control levels. (*E*–*F*″) Immunofluorescence staining of MMP-13 in vehicle control (*E*) is increased at the wound margin after amputation (*E*′) and is ubiquitous following 3 h of paclitaxel treatment (*F* and *F*′). Immunofluorescence staining of larvae transiently injected with *krt4*:dsRed in the absence of primary MMP-13 antibody (*E*″ and *F*″). (Scale bar, 50 μm.) (*G*) Mosaic keratinocyte-specific expression (red) following *krt4*:dsRed injection and MMP-13 (green) staining shows colocalization. DAPI-stained nuclei. (Scale bar, 50 μm.) (*H*) 3D rendering of one keratinocyte (red) and MMP-13 staining (green) shows colocalization. (Scale bar, 10 μm.) (*I*) 3D rendering of axons (acetylated-tubulin, green) and MMP-13 staining (red) shows no colocalization (arrows). (Scale bar, 15 μm.) (*J*–*K*″) MMP-13 staining (*J* and *K*) and axons stained with acetylated tubulin (*J*″ and *K*″) show lack of colocalization in vehicle (*J*′) and paclitaxel- (*K*′) incubated larvae. (Scale bars, 5 μm.) (*L*) Orthogonal views (sidebars) show axons (green) colocalizing with basal cell-specific MMP-13 staining (red). (*L*′ and *L*″) MMP-13 staining (arrow in *L*″) is present in the deeper basal layer below the axons (arrowhead) and is absent from the superficial periderm (*L*′). (Scale bar, 50 μm.) *P < 0.05, **P < 0.01, ***P < 0.001. AB, antibody; a.u., arbitrary units; Inj, injured; Pctx, paclitaxel; Uninj, uninjured; veh, vehicle.

addition of H_2O_2 to the larval media was ∼1.3-fold (Fig. 7 *A* and *D*). Three-hour pretreatment with paclitaxel significantly increased this ratio to ∼1.6-fold (Fig. 7 *B* and *D*). We next coadministered CL-82198, which led to decreased HyPer oxidation below levels observed when treated with DMSO vehicle (Fig. 7 *C* and *D*). Interestingly, CL-82198 administration alone led to a further reduction, suggesting either that DMSO might induce low-level MMP-13 activity or that some MMP-13 activity is necessary under homeostatic conditions to maintain the skin barrier.

To assess the role of MMP-13 in skin damage, we mechanically stressed larvae overexpressing either a wild-type homolog of MMP-13, *mmp13a*, or a mutated, nonfunctional control variant (Fig. S9 *A* and *B*) following mRNA injections into one-cell stage embryos. Mechanical stress at 2 dpf promoted rupturing of the yolk and fins in *mmp13*-overexpressing larvae, whereas larvae expressing the deletion variant were largely unaffected (Fig. 7*E*). We next tested if pharmacological MMP-13 inhibition rescued paclitaxel-dependent skin and injury phenotypes. Larvae cotreated with paclitaxel and either CL-82918 or DB04760 showed improved skin morphologies when examined with SEM (Fig. 7 *G*–*H*″ and Fig. S9*C*) and increased mechanical stress resistance (Fig. 7*F*). These findings implicate MMP-13 in paclitaxel-induced skin damage.

Increased MMP-13 Activity Impairs Wound Repair. MMP-13 is known to be up-regulated during epidermal wound repair, and we show that paclitaxel further increases MMP-13 expression upon injury (Fig. 6). We therefore assessed the relationship between paclitaxel and MMP-13 in an injury setting. We recorded 12-h time-lapse movies following puncture wounding of the caudal fin in transgenic Tg(*tp63*:CAAX-GFP) larvae in which the plasma membrane of TP63-positive basal keratinocytes is fluorescently labeled. Punctured vehicle controls showed a rapid but distinct healing response, marked by a slight increase in wound diameter within the first 2 h, followed by wound closure around 5 h (Fig. S10 *A* and *C*). Despite a similar initial wound diameter, wounds in paclitaxel-treated larvae continuously increased and failed to close (Fig. S10 *B* and *C*), which was largely rescued upon coadministration of CL-82198 and DB04760 (Fig. S10*C*).

To examine keratinocyte-specific effects, we used an established in vitro scratch assay and the human keratinocyte line HEK001 plated on a collagen matrix. We first assessed H_2O_2 production following scratch injury. Although control cells at the scratch margin produced H_2O_2 within ∼20 min (Fig. S10 *D* and *G*), which remained present until scratch wound closure was completed (Fig. S10 *D* and *E*), paclitaxel-treated keratinocytes showed a dose-dependent reduction in ROS/H_2O_2 formation during the first ∼2 h (Fig. S10 *D*′, *D*″, and *G*). At 12 h, control gaps were nearly closed and few cells produced ROS/H_2O_2, whereas gaps remained large in paclitaxel-treated wells despite the fact that many cells now produced ROS/H_2O_2 (Fig. S10 *E*, *E*′, and *H*). By 24 h, gaps were no longer visible in control wells, whereas paclitaxel impaired closure (Fig. S10 *F*, *F*′, and *H*). Thus, paclitaxel delays H_2O_2/ROS formation and impairs keratinocyte healing.

To determine the role of MMP-13 in scratch wound repair, HEK001 cells were treated with paclitaxel and either CL-82198 or DB04670 for 30 min before scratching. This showed a dose-dependent partial improvement in gap closure (Fig. S10 *I* and *J*), suggesting that impaired scratch healing is in part mediated by keratinocyte-specific MMP-13 activity. Interestingly, inhibition of MMP-13 in wild-type keratinocytes considerably enhanced scratch repair. To analyze whether closure defects were mediated by cytoskeletal defects induced by paclitaxel treatment, we monitored scratch margin cells over time (Fig. S10*K*). Although migratory control cells formed lamellipodia at the leading edges, indicating migration, lamellipodia were absent in paclitaxel-treated HEK001 cells. Coadministration of DB04760 (or CL-82198) in contrast restored lamellipodia formation and migration, as did DB04760 treatment alone. These findings indicate that increased MMP-13 activity induced by paclitaxel impairs keratinocyte migration, likely due to excessive collagen degradation.

Discussion

A roadblock in the development of therapies for paclitaxel-induced peripheral neuropathy is the lack of understanding about the underlying mechanisms. Our studies demonstrate that keratinocyte damage, which precedes axon degeneration, underlies paclitaxel

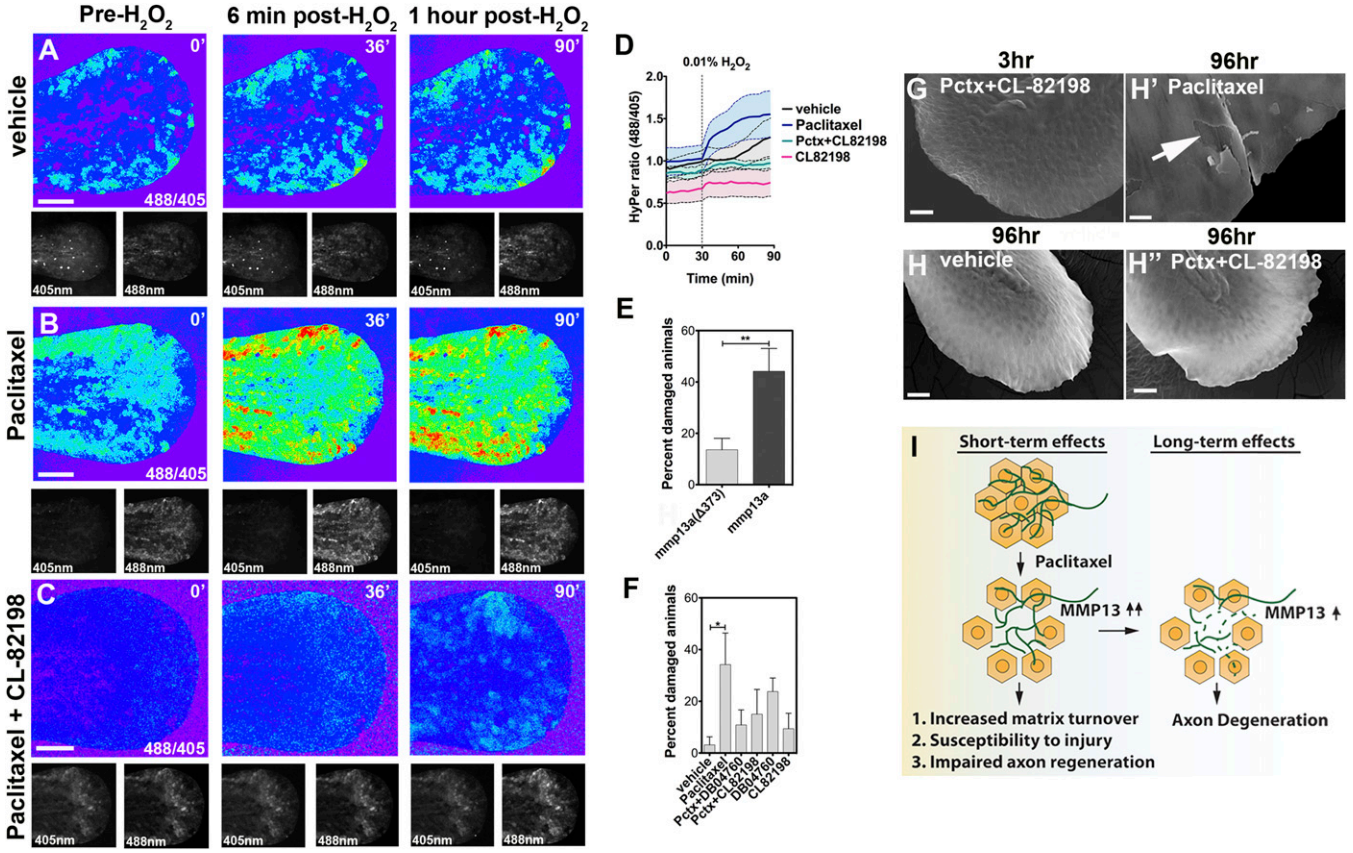

Fig. 7. Epithelial defects induced by paclitaxel are rescued upon MMP-13 inhibition. (*A–C*) Temporal sequence of HyPer oxidation in Tg(*krt4*:Gal4_tdTomato_5xUAS_HyPer) larva before and after addition of 0.01% exogenous H_2O_2 at 30 min, visualized as 488/405 nm emission ratio. Vehicle (0.5% DMSO) controls show some oxidation following H_2O_2 addition (*A*), which is increased after 3 h of paclitaxel incubation (*B*) and rescued when CL-82198 is coadministered (*C*). (Scale bar, 100 μm.) (*D*) Quantification of HyPer oxidation (n = 2, 4–5 fish per group; paclitaxel vs. paclitaxel + CL-82198; $^*P = 0.03$). (*E*) Percentage of larvae with skin damage following injection of either wild-type *mmp13a* or *mmp13a*$^{\Delta 373}$ mRNA into one-cell stage embryos and mechanical stress at 2 dpf (n = 3 biological replicates, 15 larvae per group). (*F*) Rescue of skin damage following pharmacological inhibition of MMP-13 and mechanical stress at 2 dpf (n = 3, 9–10 larvae per group). (*G–H''*) SEM of larvae incubated for 3 h in paclitaxel + CL-82198 (*G*) and 96 h in vehicle (*H*), paclitaxel (*H'*), or paclitaxel + CL-82198 (*H''*) shows improved skin morphology with CL-82198. [Scale bar, 25μm (*G*, *H*, and *H''*) and 5 μm (*H'*).] (*I*) Model of paclitaxel-induced peripheral neuropathy. Paclitaxel damages epithelial keratinocytes by up-regulating MMP-13, leading to skin damage due to increased matrix turnover and neurotoxicity. $^*P < 0.05$, $^{**}P < 0.01$. Pctx, paclitaxel.

neurotoxicity in zebrafish and that MMP-13 plays a critical role (Fig. 7*I*). This finding is intriguing, as paclitaxel-induced axon degeneration in rat models is initially evident within the epidermis (11). Why epidermal keratinocytes are affected, but not axons, is unclear. It is possible that dose-dependent differences in paclitaxel metabolism or uptake play a role. For instance, administration of paclitaxel over four cumulative doses at 2 mg/kg induced terminal arbor degeneration (TAD) in only the intraepidermal DRG axons of rats (11), which could potentially be mediated by keratinocyte-specific damage. In contrast, higher doses (>8 mg/kg) administered to rats induced distinct phenotypes, such as peripheral nerve-specific degeneration and neuronal death (43), which may relate to nerve-specific uptake of paclitaxel at high concentrations. Our model, in which we expose animals to significantly lower paclitaxel concentrations, appears to mimic more closely the TAD phenotype.

The finding that perturbations of skin homeostasis induce neurotoxicity is intriguing given that human patients undergoing chemotherapy with paclitaxel develop various skin phenotypes and wound-healing deficits (44, 45). However, data that correlate these skin phenotypes with paclitaxel-induced neuropathy are not available. Whether and how MMP-13 inhibition improves paclitaxel-induced neuropathy in humans remains to be investigated. MMP-13 is a collagenase that belongs to the MMP family of zinc-dependent neutral endopeptidases, which are matrix-degrading enzymes. Evidence suggests that general MMP inhibition using the potent MMP inhibitor tetracycline-3 positively influences paclitaxel-induced hyperalgesia in mice (46). MMPs have also been implicated in paclitaxel-induced neuropathic pain in a rat model where DRG neurons show increased expression of MMP-3 (47). Given the general role of MMPs in paclitaxel neurotoxicity, MMP-13's functions in peripheral neuropathy may not be restricted to zebrafish. The question remains by which mechanisms MMP-13 is up-regulated following paclitaxel treatment. One possibility is that MMP-13 accumulates within the ECM due to reduced protein turnover and altered microtubule functions within keratinocytes. Alternatively, microtubule stabilization alters signaling cascades that promote *mmp13a* gene expression. These could be induced by mechanical stress-dependent ROS formation. A number of factors favor this model: (*i*) We observed increased ROS/H_2O_2 formation upon mechanically stressing paclitaxel-treated zebrafish larvae; (*ii*) mechanical stress triggers Nox-2–dependent "X-ROS" formation in cardiomyocytes and skeletal myofibers (48, 49), and X-ROS formation is exacerbated in skeletal muscle of mice with Duchenne Muscular Dystrophy due to enhanced microtubule stiffness (49); and (*iii*) our RNAseq analysis shows that H_2O_2 induces *mmp13a* expression in larval zebrafish (31).

The question remains how paclitaxel and MMP-13–dependent epidermal perturbations promote axon degeneration. Excessive MMP-13 activity may lead to increased collagen degradation, which could alter the mechanical properties of the skin, given the collagen-rich network within the ECM that is essential to maintain tissue integrity (50). Because the distal fin edges and also the glabrous skin in mammals are frequently exposed to biomechanical stresses, axons in these regions may be more susceptible to damage compared with other body regions. Nociceptors and small-diameter mechanoreceptors in hairy skin have been shown to be modulated by mechanical stress through binding of collagen to integrins alpha 2 and beta 1 (12). Parallel mechanisms in glabrous skin may exist, and disruptions due to increased MMP-13 activity may promote axon degeneration. Alternatively, MMP-13 could function in cellular signaling. In the intestinal epithelium during sepsis and in inflammatory bowel disease, MMP-13 promotes LPS-induced goblet cell depletion, endoplasmic reticulum stress, and TJ destabilization through its role as TNF sheddase, which cleaves pro-TNF into its bioactive form (42). A similar function could promote junction destabilization in keratinocytes following paclitaxel treatment, consistent with reduced skin resistance and barrier function. Further studies are required to explore these possibilities. Interestingly, we observed prominent MMP-13 expression in the dermis of both adult vehicle and paclitaxel-treated animals, yet dermal axons are not affected by MMP-13 activity. One possible explanation is that the dermis contains myelinated axons which do not establish direct contact with the microenvironment, unlike unmyelinated axons in the epidermis (13, 14). This is further evidence that interactions between keratinocytes and unmyelinated axons might play a role in paclitaxel neurotoxicity in zebrafish.

Our studies demonstrated that MMP-13 inhibition with two chemical inhibitors, CL-82198 and DB04760, significantly reduced paclitaxel neurotoxicity. A number of MMP inhibitors have been developed for the treatment of cancer where MMPs are up-regulated (51). The first generation of inhibitors was designed to chelate the zinc ion in the active site, thereby preventing enzymatic activity (52). Because of the low selectivity of these inhibitors due to sequence conservation within the active site, more selective MMP inhibitors were subsequently developed. CL-82198 belongs to the class of highly selective, non–zinc-chelating compounds and was shown to exhibit specific but weak inhibition of MMP-13 (89% at 10 μg/mL) without activity against MMP-1, 9, and TACE (tumor necrosis factor-α-converting enzyme) (32). This inhibitor binds to the large S1' binding pocket without apparent interactions with the catalytic zinc binding domain, justifying its micromolar potency (32). The weak binding may be favorable in our model in that MMP-13 activity is reduced, but not abolished, to levels seen in control animals (Fig. 6*J*). Also, DB04760, a pyrimidine dicarboxamide inhibitor, belongs to the class of non–zinc-chelating, S1' pocket-binding compounds (33) and exhibited similar effects as CL-82198. Intriguingly, CL-82198 also has proven beneficial effects in decreasing cancer metastasis during which MMP-13 plays a role (53–55). MMP-13 has also been implicated in a variety of other conditions, including tendon injury and intestinal inflammatory diseases (42, 56, 57). Targeting this enzyme with these selective compounds could therefore provide multiple benefits. Intriguingly, recent data showed that paclitaxel also promotes metastasis (58), and thus, inhibitors targeting MMP-13 in neuropathy patients could provide additional benefits. Paradoxically, we found that MMP-13 inhibition of HEK001 cells promoted migration, suggesting that MMP-13 function under injury conditions may be different than in cancer. It is intriguing that in the wound setting, paclitaxel-induced cytoskeletal defects seem to be minor given that MMP-13 inhibition was able to rescue wound repair and promote HEK001 migration. Thus, paclitaxel concentrations used in our studies may primarily influence the ECM. Further studies are required to investigate the underlying basis.

Despite the fact that our findings strongly argue for epidermal influences on axons, it is possible that axons also directly uptake paclitaxel, as shown in mammalian cell culture studies (8). Although we did not detect tubulin tracker fluorescence in axons, we found it in some but not all RB cell bodies. One possibility is that only RB neurons that did not accumulate tubulin tracker innervated the caudal fin. Alternatively, tubulin tracker diffused into axons, but the concentrations were below detection limits, or rapid metabolic turnover of tubulin tracker within axons played a role. In this case, it is questionable whether such minute amounts could cause significant axon damage, a point that requires further investigation. In support of direct effects of paclitaxel is also the observation that growth cone dynamics were reduced. However, this phenotype and the lack of regenerative growth may also relate to perturbations in the ECM, leading to reduced substrate availability due to MMP-13–mediated collagen degradation. Overall, our findings argue for a primary role of epidermal damage in paclitaxel neurotoxicity, given that MMP-13 was specifically expressed in basal keratinocytes and because MMP-13 inhibition rescued short- and long-term paclitaxel neurotoxicity.

The zebrafish larval skin resembles more closely the two-layered human fetal skin (59) and is innervated by axons of trigeminal and RB neurons, as opposed to adult skin that is innervated by DRG neurons, similar to mammals. Despite this difference, RB neurons are molecularly and functionally similar to DRG (60) and trigeminal neurons (61). However, we found a less robust larval phenotype following paclitaxel injections. This could be caused by the use of pulled glass needles instead of the Hamilton syringe that we used in adults. Glass needles cannot be precisely adjusted for the injection volume and thus may have increased injection variability. Consistently, we found that some tubulin tracker-injected animals showed weak fluorescence. It is further possible that the concentration used for larval injections (10 μM) was insufficient, as we found 22 μM to be optimal for incubation studies. Thus, a higher efficacy might be achieved when injecting 22 μM, which needs to be further investigated. Also, pharmacokinetic differences in paclitaxel metabolism could play a role, which may lead to more rapid paclitaxel turnover in larvae, as these are still actively growing. Because we used single daily injections, rapid turnover would cause a less robust phenotype than seen when larvae are incubated in the drug over prolonged time periods. This model is consistent with the rapid recovery of the touch response following the last injection. Despite these differences, we detected overall similar phenotypes in larval and adult fish, also when compared with mammals, suggesting that the zebrafish is a valid model to study paclitaxel neurotoxicity.

Materials and Methods

Animals were maintained and handled in strict accordance with good animal care practices as approved by the NIH Animal Care and Use Committee and MDI Biological Laboratory Institutional Assurance #A-3562-01 under protocol #14-09. Larval paclitaxel (22 μM) incubations were performed in Ringers solution and injections (10 μM) in PBS. Adults were injected with 0.09–0.113 mg/kg paclitaxel (87–97 $\mu g/m^2$). DMSO served as control vehicle. CL-82198 (TOCRIS) and DB04760 (Santa Cruz Biotechnology) were administered at 10 μM, and DPI and Apocynin at 50 and 100 μM, respectively. For touch response, larvae were stimulated with a pipette tip at the distal tail fin until a response was observed. Adults were wrapped in plastic foil until calm, and the distal tail fin was stimulated with an insect pin until twitching of the fish was observed. For the mechanical stress assay, larvae were preexamined for injuries, and only uninjured larvae were included. Five to six larvae were gently pipetted three times with a glass Pasteur pipette and analyzed for injuries.

For more details, see *SI Materials and Methods*.

ACKNOWLEDGMENTS. We thank Drs. Gromek Smolen (Harvard University) and Chi-Bin Chien for providing reagents and Novartis for their intellectual input. We further thank Pete Finger (The Jackson Laboratory) for help with SEM and F. C. Phalan and A. M. Allen for technical support. The research was supported by IDeA Grants P20GM104318, P20GM103423, and USAMRMC-W81XWH-BAA. O.L. received a Murphy Fellowship for Biomedical Research (MDI Biological Laboratory). E.L.S., P.B.M., and E.V.C. received University of Maine GSBSE (Graduate School of Biomedical Sciences and Engineering) funding.

1. Gornstein E, Schwarz TL (2014) The paradox of paclitaxel neurotoxicity: Mechanisms and unanswered questions. *Neuropharmacol* 76(Pt A):175–183.
2. Sahenk Z, Barohn R, New P, Mendell JR (1994) Taxol neuropathy. Electrodiagnostic and sural nerve biopsy findings. *Arch Neurol* 51(7):726–729.
3. Scripture CD, Figg WD, Sparreboom A (2006) Peripheral neuropathy induced by paclitaxel: Recent insights and future perspectives. *Curr Neuropharmacol* 4(2): 165–172.
4. Argyriou AA, Koltzenburg M, Polychronopoulos P, Papapetropoulos S, Kalofonos HP (2008) Peripheral nerve damage associated with administration of taxanes in patients with cancer. *Crit Rev Oncol Hematol* 66(3):218–228.
5. Nakata T, Yorifuji H (1999) Morphological evidence of the inhibitory effect of taxol on the fast axonal transport. *Neurosci Res* 35(2):113–122.
6. Bobylev I, et al. (2015) Paclitaxel inhibits mRNA transport in axons. *Neurobiol Dis* 82: 321–331.
7. Varbiro G, Veres B, Gallyas F, Jr, Sumegi B (2001) Direct effect of Taxol on free radical formation and mitochondrial permeability transition. *Free Radic Biol Med* 31(4): 548–558.
8. Yang IH, Siddique R, Hosmane S, Thakor N, Höke A (2009) Compartmentalized microfluidic culture platform to study mechanism of paclitaxel-induced axonal degeneration. *Exp Neurol* 218(1):124–128.
9. Xiao WH, Bennett GJ (2008) Chemotherapy-evoked neuropathic pain: Abnormal spontaneous discharge in A-fiber and C-fiber primary afferent neurons and its suppression by acetyl-L-carnitine. *Pain* 135(3):262–270.
10. Dougherty PM, Cata JP, Cordella JV, Burton A, Weng HR (2004) Taxol-induced sensory disturbance is characterized by preferential impairment of myelinated fiber function in cancer patients. *Pain* 109(1-2):132–142.
11. Bennett GJ, Liu GK, Xiao WH, Jin HW, Siau C (2011) Terminal arbor degeneration—A novel lesion produced by the antineoplastic agent paclitaxel. *Eur J Neurosci* 33(9): 1667–1676.
12. Khalsa PS, Zhang C, Sommerfeldt D, Hadjiargyrou M (2000) Expression of integrin alpha2beta1 in axons and receptive endings of neurons in rat, hairy skin. *Neurosci Lett* 293(1):13–16.
13. O'Brien GS, et al. (2012) Coordinate development of skin cells and cutaneous sensory axons in zebrafish. *J Comp Neurol* 520(4):816–831.
14. Mihara M (1984) Regenerated cutaneous nerves in human epidermal and subepidermal regions. An electron microscopy study. *Arch Dermatol Res* 276(2):115–122.
15. Rieger S, Sagasti A (2011) Hydrogen peroxide promotes injury-induced peripheral sensory axon regeneration in the zebrafish skin. *PLoS Biol* 9(5):e1000621.
16. Roggenkamp D, et al. (2013) Epidermal nerve fibers modulate keratinocyte growth via neuropeptide signaling in an innervated skin model. *J Invest Dermatol* 133(6): 1620–1628.
17. Hokeness K, et al. (2005) IFN-gamma enhances paclitaxel-induced apoptosis that is modulated by activation of caspases 8 and 3 with a concomitant down regulation of the AKT survival pathway in cultured human keratinocytes. *Oncol Rep* 13(5):965–969.
18. Le Guellec D, Morvan-Dubois G, Sire JY (2004) Skin development in bony fish with particular emphasis on collagen deposition in the dermis of the zebrafish (Danio rerio). *Int J Dev Biol* 48(2-3):217–231.
19. Guzman A, Ramos-Balderas JL, Carrillo-Rosas S, Maldonado E (2013) A stem cell proliferation burst forms new layers of P63 expressing suprabasal cells during zebrafish postembryonic epidermal development. *Biol Open* 2(11):1179–1186.
20. Sun QQ, Dale N (1997) Serotonergic inhibition of the T-type and high voltage-activated Ca2+ currents in the primary sensory neurons of Xenopus larvae. *J Neurosci* 17(18):6839–6849.
21. Pittman AJ, Law MY, Chien CB (2008) Pathfinding in a large vertebrate axon tract: Isotypic interactions guide retinotectal axons at multiple choice points. *Development* 135(17):2865–2871.
22. Vaclavikova R, et al. (2004) Different in vitro metabolism of paclitaxel and docetaxel in humans, rats, pigs, and minipigs. *Drug Metab Dispos* 32(6):666–674.
23. Williams JA, et al. (2000) Programmed cell death in zebrafish rohon beard neurons is influenced by TrkC1/NT-3 signaling. *Dev Biol* 226(2):220–230.
24. Kanther M, et al. (2011) Microbial colonization induces dynamic temporal and spatial patterns of NF-κB activation in the zebrafish digestive tract. *Gastroenterology* 141(1): 197–207.
25. Gloire G, Legrand-Poels S, Piette J (2006) NF-kappaB activation by reactive oxygen species: Fifteen years later. *Biochem Pharmacol* 72(11):1493–1505.
26. Andreu JM, Barasoain I (2001) The interaction of baccatin III with the taxol binding site of microtubules determined by a homogeneous assay with fluorescent taxoid. *Biochemistry* 40(40):11975–11984.
27. Hur EM, Saijilafu, Zhou FQ (2012) Growing the growth cone: Remodeling the cytoskeleton to promote axon regeneration. *Trends Neurosci* 35(3):164–174.
28. Han C, et al. (2014) Epidermal cells are the primary phagocytes in the fragmentation and clearance of degenerating dendrites in Drosophila. *Neuron* 81(3):544–560.
29. Rasmussen JP, Sack GS, Martin SM, Sagasti A (2015) Vertebrate epidermal cells are broad-specificity phagocytes that clear sensory axon debris. *J Neurosci* 35(2):559–570.
30. Martin SM, O'Brien GS, Portera-Cailliau C, Sagasti A (2010) Wallerian degeneration of zebrafish trigeminal axons in the skin is required for regeneration and developmental pruning. *Development* 137(23):3985–3994.
31. Lisse TS, King BL, Rieger S (2016) Comparative transcriptomic profiling of hydrogen peroxide signaling networks in zebrafish and human keratinocytes: Implications toward conservation, migration and wound healing. *Sci Rep* 6:20328.
32. Chen JM, et al. (2000) Structure-based design of a novel, potent, and selective inhibitor for MMP-13 utilizing NMR spectroscopy and computer-aided molecular design. *J Am Chem Soc* 122(40):9648–9654.
33. Engel CK, et al. (2005) Structural basis for the highly selective inhibition of MMP-13. *Chem Biol* 12(2):181–189.
34. Wu N, et al. (2002) Real-time visualization of MMP-13 promoter activity in transgenic mice. *Matrix Biol* 21(2):149–161.
35. Zhang Y, et al. (2008) In vivo interstitial migration of primitive macrophages mediated by JNK-matrix metalloproteinase 13 signaling in response to acute injury. *J Immunol* 181(3):2155–2164.
36. Hattori N, et al. (2009) MMP-13 plays a role in keratinocyte migration, angiogenesis, and contraction in mouse skin wound healing. *Am J Pathol* 175(2):533–546.
37. Shindle MK, et al. (2011) Full-thickness supraspinatus tears are associated with more synovial inflammation and tissue degeneration than partial-thickness tears. *J Shoulder Elbow Surg* 20(6):917–927.
38. Yan Q, et al. (2015) The expression and significance of CXCR5 and MMP-13 in colorectal cancer. *Cell Biochem Biophys*.
39. Hillegass JM, Villano CM, Cooper KR, White LA (2007) Matrix metalloproteinase-13 is required for zebra fish (Danio rerio) development and is a target for glucocorticoids. *Toxicol Sci* 100(1):168–179.
40. Wu N, Jansen ED, Davidson JM (2003) Comparison of mouse matrix metalloproteinase 13 expression in free-electron laser and scalpel incisions during wound healing. *J Invest Dermatol* 121(4):926–932.
41. Gordon GM, et al. (2011) Comprehensive gene expression profiling and functional analysis of matrix metalloproteinases and TIMPs, and identification of ADAM-10 gene expression, in a corneal model of epithelial resurfacing. *J Cell Physiol* 226(6): 1461–1470.
42. Vandenbroucke RE, et al. (2013) Matrix metalloproteinase 13 modulates intestinal epithelial barrier integrity in inflammatory diseases by activating TNF. *EMBO Mol Med* 5(7):932–948.
43. Peters CM, et al. (2007) Intravenous paclitaxel administration in the rat induces a peripheral sensory neuropathy characterized by macrophage infiltration and injury to sensory neurons and their supporting cells. *Exp Neurol* 203(1):42–54.
44. Colson F, et al. (2013) Paclitaxel-related lymphedema and scleroderma-like skin changes. *J Clin Case Rep* 3(11):1–4.
45. Poi MJ, et al. (2013) Docetaxel-induced skin toxicities in breast cancer patients subsequent to paclitaxel shortage: A case series and literature review. *Support Care Cancer* 21(10):2679–2686.
46. Parvathy SS, Masocha W (2013) Matrix metalloproteinase inhibitor COL-3 prevents the development of paclitaxel-induced hyperalgesia in mice. *Med Princ Pract* 22(1): 35–41.
47. Nishida K, et al. (2008) Up-regulation of matrix metalloproteinase-3 in the dorsal root ganglion of rats with paclitaxel-induced neuropathy. *Cancer Sci* 99(8):1618–1625.
48. Prosser BL, Ward CW, Lederer WJ (2011) X-ROS signaling: Rapid mechano-chemo transduction in heart. *Science* 333(6048):1440–1445.
49. Kerr JP, et al. (2015) Detyrosinated microtubules modulate mechanotransduction in heart and skeletal muscle. *Nat Commun* 6:8526.
50. Kolácná L, et al. (2007) Biochemical and biophysical aspects of collagen nanostructure in the extracellular matrix. *Physiol Res* 56(Suppl 1):S51–S60.
51. Hidalgo M, Eckhardt SG (2001) Development of matrix metalloproteinase inhibitors in cancer therapy. *J Natl Cancer Inst* 93(3):178–193.
52. Vandenbroucke RE, Libert C (2014) Is there new hope for therapeutic matrix metalloproteinase inhibition? *Nat Rev Drug Discov* 13(12):904–927.
53. Rath T, et al. (2011) Matrix metalloproteinase-13 is regulated by toll-like receptor-9 in colorectal cancer cells and mediates cellular migration. *Oncol Lett* 2(3):483–488.
54. Airola K, et al. (1999) Expression of collagenases-1 and -3 and their inhibitors TIMP-1 and -3 correlates with the level of invasion in malignant melanomas. *Br J Cancer* 80(5-6):733–743.
55. Holtkamp N, et al. (2007) MMP-13 and p53 in the progression of malignant peripheral nerve sheath tumors. *Neoplasia* 9(8):671–677.
56. Wang M, et al. (2013) MMP13 is a critical target gene during the progression of osteoarthritis. *Arthritis Res Ther* 15(1):R5.
57. Holtkamp N, et al. (2004) Differentially expressed genes in neurofibromatosis 1-associated neurofibromas and malignant peripheral nerve sheath tumors. *Acta Neuropathol* 107(2): 159–168.
58. Volk-Draper L, et al. (2014) Paclitaxel therapy promotes breast cancer metastasis in a TLR4-dependent manner. *Cancer Res* 74(19):5421–5434.
59. Pellegrini G, et al. (2001) p63 identifies keratinocyte stem cells. *Proc Natl Acad Sci USA* 98(6):3156–3161.
60. Faucherre A, Nargeot J, Mangoni ME, Jopling C (2013) piezo2b regulates vertebrate light touch response. *J Neurosci* 33(43):17089–17094.
61. Palanca AM, et al. (2013) New transgenic reporters identify somatosensory neuron subtypes in larval zebrafish. *Dev Neurobiol* 73(2):152–167.
62. Lisse TS, Brochu EA, Rieger S (2015) Capturing tissue repair in zebrafish larvae with time-lapse brightfield stereomicroscopy. *J Vis Exp* 95:1–9.